Intel Serv Robotics (2015) 8:215–224
DOI 10.1007/s11370-015-0180-3

ORIGINAL RESEARCH PAPER

Practical analytical inverse kinematic approach for 7-DOF space manipulators with joint and attitude limits

Dongsheng Zhou[1] · **Lu Ji**[1] · **Qiang Zhang**[1] · **Xiaopeng Wei**[2]

Received: 3 February 2015 / Accepted: 8 June 2015 / Published online: 30 June 2015

Abstract In this study, we propose a practical approach for calculating the analytical inverse kinematic solution for a seven-degrees of freedom (7-DOF) space manipulator with joint and attitude limits. Instead of utilizing traditional velocity-based approaches that limit the ranges of joints by calculating the velocity-level Jacobian matrix, we propose a position-based approach for evaluating the ranges of feasible inverse kinematic solutions. We then search for the optimal solution, which is estimated based on the disturbance that acts on the base of the manipulator to obtain the final solution. First, the concept of the redundancy of manipulators is defined and each joint is parameterized by the redundancy. Second, how the joint limits affect this redundancy is discussed. Third, a practical approach (include the objective function that the author needs to minimize) is proposed for dealing with the inverse kinematic problem of 7-DOF manipulators. Finally, the validity of this approach is verified by numerical simulation.

Keywords Analytical inverse kinematic · 7-DOF redundant manipulator · Joint limit · Minimal base disturbance · Space manipulator

✉ Dongsheng Zhou
donyson@126.com

Qiang Zhang
zhangq@dlu.edu.cn

[1] Key Laboratory of Advanced Design and Intelligent Computing, Ministry of Education, Dalian University, Dalian 116622, China

[2] School of Mechanical Engineering, Dalian University of Technology, Dalian 116024, China

1 Introduction

In the short history of research into redundant manipulators, an analytical inverse kinematic solution for a redundant manipulator is generally regarded as a difficult problem because no inverse kinematic solution can be determined even if the end-effector has already been fixed in an unchanged pose. Furthermore, the attitude and position of the base of space manipulators can be affected by the motion of manipulators [1]. Traditionally, the solution to the problem of the control of manipulators with joint and attitude has been limited to velocity-level approaches, such as those proposed in [2] or [3]. However, the velocity-level solution hardly retains the characteristics of the multi-solution of the inverse kinematics for redundant manipulators. Thus, there is a need for an analytical inverse kinematic approach, which has already attracted the attention of some researchers, although this problem is difficult. Lee and Bejczy [4] proposed a method for calculating a closed-form inverse solution for DOF manipulators, although the selection of parameters is quite difficult and the joint limits are not considered. Previous studies [5,6] also discussed how the shoulder limits and the wrist limits affect the inverse solution, but the self-motion of manipulators was ignored. Asfour and Dillmann [7] also proposed an inverse kinematic algorithm for a humanoid robot arm, but they did not analyze the joint limits. Shimizu [8] derived a fairly complete method for handling this problem, which was developed further [9]. However, this approach can only be utilized on the ground. A summary of various methods can be found in [10–13].

In the present study, the approach proposed in [9] is extended to a more general case, particularly in the environment of space, which is completely different from the ground in a conceptual sense. The types of singularity are discussed comprehensively and clearly, while a useable process is pro-

posed for handling practical applications. Finally, we tested some more general samples rather than specific ones to verify the validity of this algorithm.

2 Modeling and parameterization

There are four general types of seven-degrees of freedom (7-DOF) redundant manipulators, i.e., SRS (Sphere-Rotation-Sphere), RSS (Rotation-Sphere-Sphere), UUS-A (Universe-Universe-Sphere A type), and UUS-B (Universe-Universe-Sphere B type) [14], but our approach can only be applied to the SRS structure. Hollerbach [15] also showed that the SRS model is the optimal model of 7-DOF manipulators. As shown in Fig. 1, SRS manipulators comprise seven revolute joints and the links between them, which are generally regarded as the shoulder (joints 1, 2 and 3), elbow (joint 4), wrist (joints 5, 6, and 7), upper arm (base-proximal link), and forearm (base-distal link) joints. The shoulder joint is equal to a virtual spherical joint because the joint axes intersect at a single point. The wrist joint possesses the same features as the shoulder joint.

To describe the direct kinematics of a manipulator, we define the coordinate systems as follows. First, $\sum_{\mathbf{0}}$ is the base coordinate system, $\sum_i$ $(i = 1, \ldots, 7)$ is defined based on Table 1, and $\sum_7$ is placed on the end-effector (or tip). Second, the origin of $\sum_i$ is fixed on the joint $i + 1$, where its z-axis is aligned with its joint axis, its x-axis is aligned with the common normal to the joint axes i and $i + 1$, and its y-axis is limited by the "right-hand rule." Finally, when $\theta_1 = 0$, $\sum_{\mathbf{0}}$ coincides with $\sum_{\mathbf{1}}$. All of the joints are arranged in a straight line and the end-effector arrives at the edge of the workplace when all of the joint angles are zero.

Because 7-DOF is a type of redundant structure of manipulators, a parameter is required that can be used to describe the redundant DOFs. There are several methods for dealing with this, i.e., Lee and Bejczy [4] proposed an approach for representing the redundancy of manipulators, Tondu [16] suggested that joints 1 and 3 appear to be the best choices for parameterizing the redundancy, and Yu [17] utilized joint 7 as the redundant joint. However, it is not possible to uniquely determine the redundant joint angle based on other joints because there are nonlinear relationships between the joints of 7-DOF manipulators. A previous study [15] also addressed the concept of "self-motion," i.e., the upper arm and the forearm can revolve around the line between the shoulder and wrist even if the position and orientation of the end-effector are fixed. As shown in Fig. 2, the reference plane is determined by the upper arm and forearm when joint 3 is zero (at this point, the manipulator is equal to a 6-DOF manipulator and the reference plane is unique). As defined above, the plane of the upper arm and forearm can rotate around the axis fixed by the shoulder and wrist. After rotation, the new plane is called the arm plane and ψ is used to define the angle of the distance between these two planes: the *arm angle*. Therefore, we can represent the rotation matrix of each joint in the following form:

$$\begin{aligned} {}^{b}\boldsymbol{R}_{s} &= {}^{0}\boldsymbol{R}_{1} \cdot {}^{1}\boldsymbol{R}_{2} \cdot {}^{2}\boldsymbol{R}_{3} \\ {}^{s}\boldsymbol{R}_{e} &= {}^{3}\boldsymbol{R}_{4} \\ {}^{e}\boldsymbol{R}_{t} &= {}^{4}\boldsymbol{R}_{5} \cdot {}^{5}\boldsymbol{R}_{6} \cdot {}^{6}\boldsymbol{R}_{7}. \end{aligned} \tag{2.1}$$

Table 1 D-H parameters

i	α_{i-1} (rad)	a_{i-1}	d_i	θ_i
1	$-\pi/2$	0	d_{bs}	θ_1
2	$\pi/2$	0	0	θ_2
3	$-\pi/2$	0	d_{se}	θ_3
4	$\pi/2$	0	0	θ_4
5	$-\pi/2$	0	d_{ew}	θ_5
6	$\pi/2$	0	0	θ_6
7	0	0	d_{wt}	θ_7

Fig. 1 7-DOF manipulator model

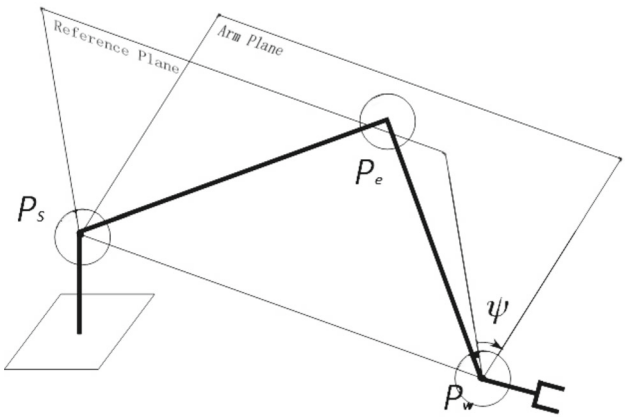

Fig. 2 Schematic of the 7-DOF structure

where

$$ {}^{i-1}\boldsymbol{R}_i = \begin{bmatrix} \cos\theta_i & -\sin\theta_i \cdot \cos\alpha_{i-1} & \sin\theta_i \cdot \sin\alpha_{i-1} \\ \sin\theta_i & \cos\theta_i \cdot \cos\alpha_{i-1} & -\cos\theta_i \cdot \sin\alpha_{i-1} \\ 0 & \sin\alpha_{i-1} & \cos\alpha_{i-1} \end{bmatrix}. $$

The position and orientation of the end-effector (tip) is represented as

$$ \begin{aligned} {}^b\boldsymbol{x}_t &= {}^b\boldsymbol{l}_{bs} + {}^b\boldsymbol{R}_s \cdot [{}^s\boldsymbol{l}_{se} + {}^s\boldsymbol{R}_e \cdot ({}^e\boldsymbol{l}_{ew} + {}^e\boldsymbol{R}_w \cdot {}^w\boldsymbol{l}_{wt})] \\ {}^b\boldsymbol{R}_t &= {}^b\boldsymbol{R}_s \cdot {}^s\boldsymbol{R}_e \cdot {}^e\boldsymbol{R}_t. \end{aligned} \tag{2.2} $$

The position of the wrist is unchanged when the posture of the end-effector is fixed. Therefore, we can calculate the angle of the elbow using the Law of Cosines. Obviously, the elbow only contains joint 4, so θ_4 is given by

$$ \theta_e = \theta_4 = \text{acos}\frac{\|{}^b\boldsymbol{x}_{sw}\|^2 - d_{se}^2 - d_{ew}^2}{2 \cdot d_{se} \cdot d_{ew}}. \tag{2.3} $$

We can obtain two solutions from (2.3), but one is redundant due to the self-motion of manipulators and only the positive value is needed.

We can obtain the equations for $\theta_1, \theta_2, \theta_3$ by calculating $\tan\theta_1 = {}^b\boldsymbol{R}_s(2,2)/{}^b\boldsymbol{R}_s(1,2)$, $\cos\theta_2 = -{}^b\boldsymbol{R}_s(3,2)$, $\tan\theta_3 = -{}^b\boldsymbol{R}_s(3,3)/{}^b\boldsymbol{R}_s(3,1)$, and we have

$$ \begin{aligned} \theta_1 &= \text{atan2}\,(-a_{s22} \cdot \sin\psi - b_{s22} \cdot \cos\psi - c_{s22}, \\ &\quad -a_{s12} \cdot \sin\psi - b_{s12} \cdot \cos\psi - c_{s12}) \\ \theta_2 &= \text{acos}\,(-a_{s32} \cdot \sin\psi - b_{s32} \cdot \cos\psi - c_{s32}), \\ \theta_3 &= \text{atan2}\,(a_{s33} \cdot \sin\psi + b_{s33} \cdot \cos\psi + c_{s33}, \\ &\quad -a_{s31} \cdot \sin\psi - b_{s31} \cdot \cos\psi - c_{s31}), \end{aligned} \tag{2.4} $$

where $a_{sij}, b_{sij}, c_{sij}$ are the (i, j) elements of $\boldsymbol{A}_s, \boldsymbol{B}_s, C_s$, respectively. $\boldsymbol{A}_s = {}^b\tilde{\boldsymbol{u}}_{sw} \cdot {}^b\boldsymbol{R}_s|_{\psi=0}$, $\boldsymbol{B}_s = -{}^b\tilde{\boldsymbol{u}}_{sw}^2 \cdot {}^b\boldsymbol{R}_s|_{\psi=0}$, $\boldsymbol{C}_s = {}^b\boldsymbol{u}_{sw} \cdot {}^b\boldsymbol{u}_{sw}^T \cdot {}^b\boldsymbol{R}_s|_{\psi=0}$ (note that if ${}^b\tilde{\boldsymbol{u}}_{sw}$ is the skew-symmetric matrix of ${}^b\boldsymbol{u}_{sw}$, which denotes the unite vector ${}^b\boldsymbol{x}_{sw}$). Similarly, we get the last three joints:

$$ \begin{aligned} \theta_5 &= \text{atan2}\,(a_{w23} \cdot \sin\psi + b_{w23} \cdot \cos\psi + c_{w23}, a_{w13} \cdot \sin\psi \\ &\quad + b_{w13} \cdot \cos\psi + c_{w13}) \\ \theta_6 &= \text{acos}\,(a_{w33} \cdot \sin\psi + b_{w33} \cdot \cos\psi + c_{w33}) \\ \theta_7 &= \text{atan2}\,(a_{w32} \cdot \sin\psi + b_{w32} \cdot \cos\psi + c_{w32}, \\ &\quad - a_{w31} \cdot \sin\psi - b_{w31} \cdot \cos\psi - c_{w31}), \end{aligned} \tag{2.5} $$

where $\boldsymbol{A}_w = {}^s\boldsymbol{R}_e^T \cdot \boldsymbol{A}_s^T \cdot {}^b\boldsymbol{R}_t$, $\boldsymbol{B}_w = {}^s\boldsymbol{R}_e^T \cdot \boldsymbol{B}_s^T \cdot {}^b\boldsymbol{R}_t$, $\boldsymbol{C}_w = {}^s\boldsymbol{R}_e^T \cdot \boldsymbol{C}_s^T \cdot {}^b\boldsymbol{R}_t$.

At this point, we have already parameterized $\theta_1, \theta_2, \theta_3, \theta_5, \theta_6, \theta_7$ by ψ and θ_4 is unrelated to ψ.

3 Inverse kinematic solution with joint limits

For various reasons, such as obstacles caused by the structure of the manipulators and cables, each joint must satisfy a range that prevents it from reaching the edge of the workplace. Based on the discussion above, we already know that ψ is the only parameter of θ_i. Now, we will analyze how the limits of the joints affect ψ.

From (2.4) and (2.5), we can note that there are only two types of relationship between θ_i and ψ when joints are rotating, i.e., Tan Type and Cos Type, and in Fig. 3 we illustrate all of them.

The difference between Fig. 3b and a is worthy of note, i.e., the center of asymmetry of Fig. 3b does not coincide

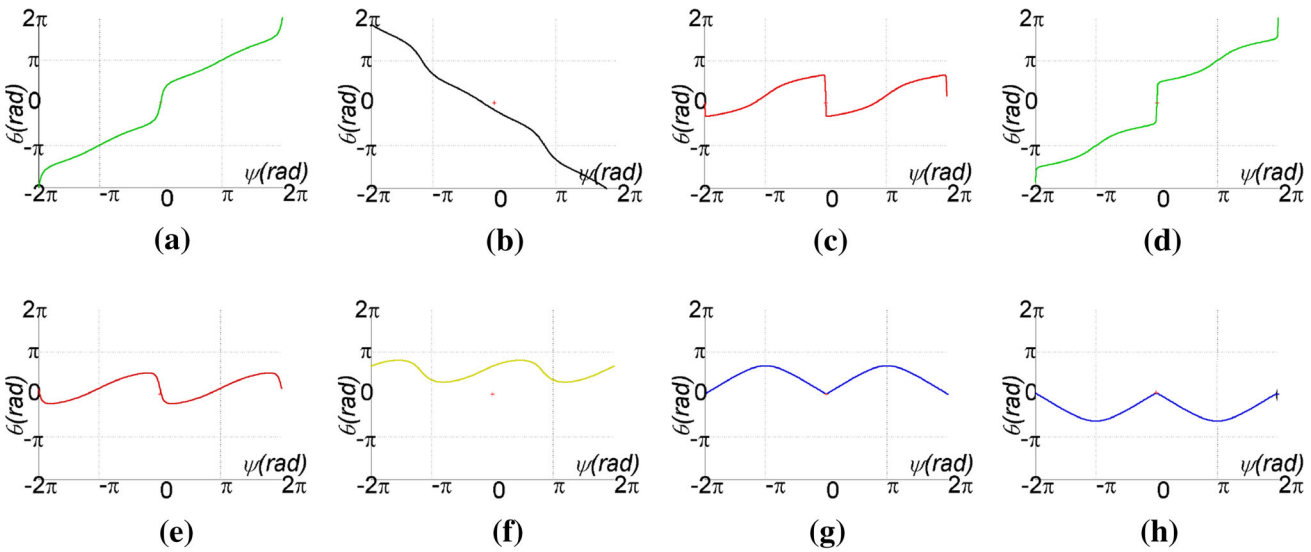

Fig. 3 Profiles of the relationships between θ_i and ψ in different cases **a** monotonic-1 **b** monotonic-2 **c** Tan singular-1 **d** Tan singular-2 **e** Tan cyclic-1 **f** Cos cyclic-1 **g** Cos singular-1 **h** Cos singular-2

with (0, 0), whereas the center of asymmetry of Fig. 3a does coincide with (0, 0). Indeed, the profiles of the equations for joints 5, 6, and 7 all share this feature, whereas the profiles of the equations for joints 1, 2, and 3 lack this feature. We can simply determine the axis of symmetry as follows:

$$\begin{aligned} \text{eul} &= \text{dc2eul}({}^{b}\boldsymbol{R}_t) \\ \text{axis} &= -\frac{\text{eul}_y}{\text{abs}(\text{eul}_y)} \cdot (\pi - \text{eul}_y). \end{aligned} \tag{3.1}$$

First, we convert the orientation of the end-effector from the rotation matrix to Z–Y–Z Eulerian angles and then calculate the arc of the y-axis with respect to the z-axis of the base coordinate system.

We divide the relationships between ψ and $\theta_1, \theta_2, \theta_3, \theta_5, \theta_6, \theta_7$ into three types, i.e., monotonic (contains tan type only), cyclic (contains tan type and cos type), and singular types (contains tan type and cos type), and each type will affect the value of arm angle.

Monotonic type: In this case, the one-to-one correspondence between θ_i and ψ is clear; thus we can get the unique ψ^u and ψ^l, respectively, which are the upper limit and lower limit of ψ, $\psi = [\psi^l, \psi^u]$.

Cyclic type: In this case, when $\theta_i^u > \theta_i^{\max}$ or $\theta_i^l < \theta_i^{\min}$, there are only two values of ψ, i.e., ψ^u and ψ^l, so we can ensure that the value of θ_i attains its extremum. However, when $\theta_i^u < \theta_i^{\max}$ or $\theta_i^l > \theta_i^{\min}$, two different values correspond to ψ^u or ψ^l. Usually we can obtain a continuous or separate range from the intersection of all of the ranges above, where this range is a set of feasible values of ψ, which that can ensure that each joint satisfies its boundary.

Singular type: To achieve our aims, all types of singularity are discussed in this section. First, we roughly classify the singularities into three types: kinematic singularity [18], algorithm singularity, and semisingularity [19]:

(1) For 7-DOF kinematics, the kinematic singularity comprises the shoulder, elbow, and wrist singularity, where the elbow and wrist singularities have no effects on manipulators. However, when a shoulder singularity occurs, the value of joint 1 cannot be determined because the result from the wrist lies on the extended line of the joint axis 1. At this point, we can only assign a value of zero to joint 1.

(2) Algorithm singularity: As described by (2.4–2.5) each of joint angles can express the equations of $\theta_1, \theta_3, \theta_5, \theta_7$ as implicit function form:

$$\tan\theta_i = \frac{a_n \cdot \sin\psi + b_n \cdot \cos\psi + c_n}{a_d \cdot \sin\psi + b_d \cdot \cos\psi + c_d}. \tag{3.2}$$

or

$$\cos\theta_i = a \cdot \sin\psi + b \cdot \cos\psi + c. \tag{3.3}$$

At the beginning of this section, we confirmed this condition by noting that $a^2 + b^2 - (c-1)^2 = 0$ or $a^2 + b^2 - (c+1)^2 = 0$, and $a_t^2 + b_t^2 - c_t^2 = 0$ for the cos type and tan type, respectively, where $a_t = b_d c_n - b_n c_d$, $b_t = a_n c_d - a_d c_n$, $c_t = a_n b_d - a_d b_n$.

From Fig. 3g, h, for the cos type, we can usually determine a unique value of θ_i even if ψ attains the singular point. The left-hand and right-hand limit can help to ensure this, although the value of θ_i cannot be calculated directly at the point of singularity [9]. In addition, the cos singular type shares similar features with the cyclic type.

However, the tan singular type possesses some quite different features compared with the cyclic type because the value of θ_i can be uniquely determined for any ψ as a monotonic type, except ψ can achieve the singular point. Thus, we should separate this point from the range of ψ.

(3) Semi algorithm singularity (SAS): SAS is a kind of algorithm singularity. It occurs when the joints reach the position limits. While it is more difficult to be solved than the kinematics singularity. In order to avoid the problem of SAS, a simple unary optimization algorithm is adopted to solve the kinematics inverse solution. And the solution is away from every joint limit.

First of all, the value of arm angle meeting their respective joint limit is determined, which is through the methods described above. That is to say, it is just to take intersection in the range of arm angle. However, there still exists the possibility that the range of arm angle makes one joint or more approach to the limits of their own. It may cause the SAS, while this is not to be expected. In this paper, $\theta_i^d = (\theta_i^l + \theta_i^u)/2$ represents the every expected joint value. Thus, ${}^{b}\boldsymbol{R}_s^d$ represents the rotation matrix of expected shoulder joint, and ${}^{e}\boldsymbol{R}_t^d$ represents the rotation matrix of expected wrist joint. The actual ${}^{b}\boldsymbol{R}_s$ and ${}^{e}\boldsymbol{R}_t$ can be regarded as the expected shoulder and wrist joint if they are at a minimum distance. To the greatest extent, it is away from the joint limit. According to the generalized rotation matrix, if $\boldsymbol{R}$ is the actual rotation matrix and $\boldsymbol{R}^d$ is the expected rotation matrix, $\boldsymbol{R} \cdot \boldsymbol{R}^{dT}$ is closer to the unit matrix $\boldsymbol{I}_3$. What is more, the direction is much closer expressed by the two rotation matrix.

Generally, a certain angle of rotation around an axis could be expressed as an arbitrary rotation matrix. The difference between the actual and expected direction can be expressed as the following formula:

$${}^{b}\boldsymbol{R}_s \cdot {}^{b}\boldsymbol{R}_s^{dT} = \boldsymbol{I}_3 + \sin\phi_s \cdot {}^{b}\tilde{\boldsymbol{u}}_s + (1 - \cos\phi_s) \cdot {}^{b}\tilde{\boldsymbol{u}}_s^2 \tag{3.4}$$

The trajectory of matrix can be expressed as the following formula:

$$\begin{aligned} f_s(\psi) &= \text{trace}({}^{b}\boldsymbol{R}_s \cdot {}^{b}\boldsymbol{R}_s^{dT}) = a_s \cdot \sin\psi + b_s \cdot \cos\psi + c_s \\ &= 1 + 2 \cdot \cos\phi_s, \end{aligned} \tag{3.5}$$

where $a_s = \text{trace}(\boldsymbol{A}_s \cdot {}^b\boldsymbol{R}_s^{dT})$, $b_s = \text{trace}(\boldsymbol{B}_s \cdot {}^b\boldsymbol{R}_s^{dT})$, $c_s = \text{trace}(\boldsymbol{C}_s \cdot {}^b\boldsymbol{R}_s^{dT})$.

It can be obviously seen that the maximum of $f_s(\psi)$ is 3. So the value is more close to 3, and the three actual joints are more far away from the joint limits. The ψ can be solved when the $f_s(\psi)$ obtains the maximum value through the following formula (derived from (2.4)):

$$\psi_s^{\mp} = 2 \cdot \text{atan}\frac{-b_s \mp \sqrt{a_s^2 + b_s^2}}{a_s} \tag{3.6}$$

The $f_s(\psi)$ must be in one of the two results, which are solved by the above formula. This ψ_s is the best value for the shoulder joint which can be denoted by ψ_s^{opt}. It is the least likely to make the SAS of shoulder joint. However, the ψ_s^{opt} may be out of the range of arm angle. In this case, one of the most close to the ψ_s^{opt} is selected as the value. It is the same as solutions of the ψ_w^{opt} and ψ_g^{opt}. Besides, the ψ_w^{opt} of wrist can be determined by the same theory. Next, it is considered that the impact for the global optimal ψ_g^{opt} which is caused by the comprehensive results from shoulder and wrist joints. It is can be simply calculated by the following formula:

$$\psi^{\mp} = 2 \cdot \text{atan}\frac{-b \mp \sqrt{a^2 + b^2}}{a}, \tag{3.7}$$

where $a = (a_s + a_w)/2$, $b = (b_s + b_w)/2$.

In the end, the global optimal ψ_g^{opt} is taken to the formulas (2.4) and (2.5). Then the value of joint will be obtained, which is farthest away from their respective joint limit.

4 Selecting the optimized arm angle

Now, we have all of the feasible values of ψ, so we hope that every joint angle is as close as possible to its desired angle, thereby ensuring that the base of the manipulators experiences the minimum disturbance. Therefore, we need clear criteria for evaluating the degree of base attitude disturbance for space manipulators so we can select a unique solution for the arm angle that corresponds to the minimal base disturbance. In this study, the error quaternions have a significant role as a minimal set for describing the orientation of a rigid arm after finite rotations, which correspond to its rotational transformation matrix [20]. A quaternion equation is defined as follows:

$$\boldsymbol{Q} = \eta + q_1\vec{i} + q_2\vec{j} + q_3\vec{k} = \eta + \boldsymbol{q} \in R^4. \tag{4.1}$$

It has one constraint equation:

$$\eta^2 + q_1^2 + q_2^2 + q_3^2 = 1 \tag{4.2}$$

We can establish the relationship between the time differentiation of the quaternion and the angular velocity ω:

$$\begin{bmatrix} \dot{\eta} \\ \dot{\boldsymbol{q}} \end{bmatrix} = \frac{1}{2}\begin{bmatrix} 0 & -\omega^T \\ \omega & -\tilde{\omega} \end{bmatrix}\begin{bmatrix} \eta \\ \boldsymbol{q} \end{bmatrix} = \frac{1}{2}\begin{bmatrix} -\boldsymbol{q}^T \\ \eta\boldsymbol{E} - \tilde{\boldsymbol{q}} \end{bmatrix}\omega. \tag{4.3}$$

The orientation error is given by $\delta\eta$, $\delta\boldsymbol{q}$ [21]

$$\begin{cases} \delta\eta = \eta_{b0}\eta_{bf} + \boldsymbol{q}_{b0}^T\boldsymbol{q}_{bf} \\ \delta\boldsymbol{q} = \eta_{b0}\boldsymbol{q}_{bf} - \eta_{bf}\boldsymbol{q}_{b0} - \tilde{\boldsymbol{q}}_{b0}\boldsymbol{q}_{bf} \end{cases}, \tag{4.4}$$

where $\delta\boldsymbol{q}$ is a single value, which can express the degree of attitude disturbance of space manipulators, and ω is calculated from the standard GJM (generalized Jacobian matrix) equation, as follows:

$$\boldsymbol{J}^*(\boldsymbol{\Psi}_b, \boldsymbol{\Theta}, m_i, \boldsymbol{I}_i). \tag{4.5}$$

Many basic concepts and definitions need to be discussed if we want to understand the entire entry for GJM in a comprehensive manner, but there is insufficient space in this article. Thus, referring to previous studies [22–24] may be helpful. However, we note that the GJM can build a bridge between the base attitude of manipulators ($\boldsymbol{\Psi}_b$) and the degree of every joint ($\boldsymbol{\Theta}$) because the other two parameters are constant, which refer to the mass and inertia matrix of the links, respectively. In short, we introduce the dynamic parameters of the manipulators using the GJM method and only check the feasible arm angle (ψ) to determine whether it can satisfy the request to minimize the disturbance of the base of space manipulators. Compared with existing methods [3,24], the proposed approach can increase the efficiency of planning by 100 times or more.

A summary of the approach is as follows:

Step 1: Calculate the position of the wrist with respect to the base coordinate system and joint 4.
Step 2: Calculate ${}^b\boldsymbol{R}_s\big|_{\psi=0}$ and the parameters.
Step 3: Detect the types of joints.
Step 4: Calculate the ranges of the feasible arm angles ψ and revise them to satisfy the limits of the joints.
Step 5: Determine the intersection of every feasible range of ψ and separate the singular point from this set.
Step 6: Select an optimal solution that can makes $\delta\boldsymbol{q}$ as close to zero as possible using the traditional method so the speed of the joints satisfies the *Trapezoidal Planning Law*.

5 The determination of arm-length and joint limits

In the S-R-S space manipulator, the working space is determined by the length of upper arm and forearm [25]. Hence,

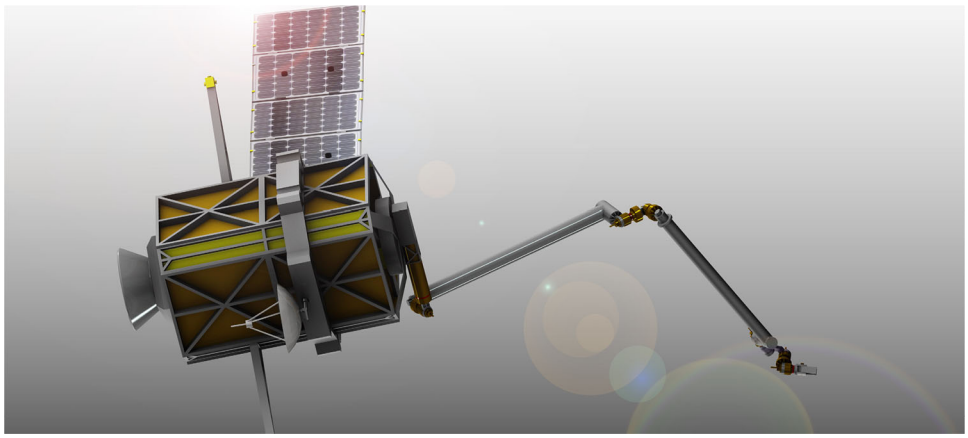

Fig. 4 Impression drawing of the 7-DOF space manipulator

the length of l_2 and l_4 can be determined when the operation space of end manipulator is known. From the Fig. 2, it is can be seen that the length of l_2 and l_4 is only related to the joint 4 with the certain working space of manipulator. While the determination of joint 3 is at least considering three factors: (1) the angle of joint 4 should be as far as possible close to the position of reasonable stress; (2) keeping away from the singular point and limit; (3) as far as possible to make the working space of manipulator large. In this paper, joint 4 has been analyzed. The singular points of joint 4 are only 0° and 180°. Because joint 4 has two solutions, we only take values among the range of 0°–180°. In order to ensure the strength of joint 4, its value should be far away from the 30° of singular points. At the same time, it as far as possible maintains the large range of working space. That is why the range limit of joint 4 is among the 30°–150°. And the other joints should be far away from the 10° of singular points.

6 Simulations

This study is a basic research component of a national space manipulators project. To verify the suitability of the methods proposed earlier, it will be applied to 7-DOF space manipulators in a microgravity environment, as shown in Fig. 4, where the kinematics are similar to the structure in Fig. 1. In the task that needs to be simulated, the end-effector must handle equipment while attached to a satellite carrier, which is a typical task for space manipulators. Some of the parameters related to the manipulators are shown in Tables 2 and 3.

The simulation environment is MATLAB 2013a using the toolbox "*Spacedyn*" programmed by Shimizu et al. [26]. The parameters of the 7-DOF manipulator which are related to Table 1 are as follows:

$$d_{bs} = 0.13\ \text{m}\ d_{se} = 1.62\ \text{m}\ d_{ew} = 1.46\ \text{m}\ d_{wt} = 0.08\ \text{m}.$$

The entire mass of the system (base satellite and manipulators) is 1146.347 kg and the position of the base with respect to the center of mass of the satellite is [0 0.850 0.476](m). The inertia matrix of the satellite and its base is expressed as an entire matrix, as follows:

Table 2 Limitations of each joint

i	1	2	3	4	5	6	7
θ_i^l (°)	−170	−150	−150	30	−170	−170	−170
θ_i^u (°)	170	150	150	150	170	170	170

$$\boldsymbol{I}_0 = \begin{bmatrix} 291.1 & 10.16 & -25.15 \\ 10.16 & 536.3 & -4.100 \\ -25.15 & -5.000 & 669.6 \end{bmatrix}.$$

Suppose that the total running, acceleration, and deceleration durations are 20, 3, and 3 s, respectively, and that the desired attitude and position of the end-effector of the manipulator with respect to the center of mass of the satellite is specified by

$$\boldsymbol{T}_d = \begin{bmatrix} 0.105 & 0.824 & 0.557 & 1.500 \\ 0.653 & 0.365 & -0.663 & 1.200 \\ -0.750 & 0.433 & -0.500 & 0.700 \\ 0 & 0 & 0 & 1 \end{bmatrix}.$$

The set of feasible values of ψ limited by each joint calculated using the proposed method is as follows:

$$\begin{aligned} &\psi_1 \in [\,-180\ 180\,]^\circ \\ &\psi_2 \in [\,-180\ 180\,]^\circ \\ &\psi_3 \in [\,-159.454\ 159.454\,]^\circ \\ &\psi_4 \in [\,-180\ 180\,]^\circ \\ &\psi_5 \in [\,-180\ 116.769\,]^\circ \\ &\psi_6 \in [\,-180\ 180\,]^\circ \\ &\psi_7 \in [\,-180\ -38.236\,] \cup [\,32.140\ 180\,]^\circ. \end{aligned}$$

The final feasible region of ψ is the intersection of above regions. Computing the intersection yields

Table 3 Mass properties of each body

	l_1	l_2	l_3	l_4	l_5	l_6	l_7
m (kg)	3.691	60.416	3.678	35.653	3.460	2.624	0.113
l (m)	0.130	1.500	0.120	1.240	0.220	0.070	0.010
I_{xx} (kg m^2)	0.013	13.556	0.012	1.235	0.0619	0.006	2.55e−05
I_{yy} (kg m^2)	0.005	2.274	0.010	7.309	0.028	0.004	2.55e−05
I_{zz} (kg m^2)	0.015	15.756	0.005	6.104	0.035	0.004	4.92e−05
$*$	I_{xy} −0.003	I_{xy} 0.155	I_{xy} 2.274	I_{yz} − 0.003	I_{xz} / I_{zx} − 0.003	I_{zy} − 0.024	0

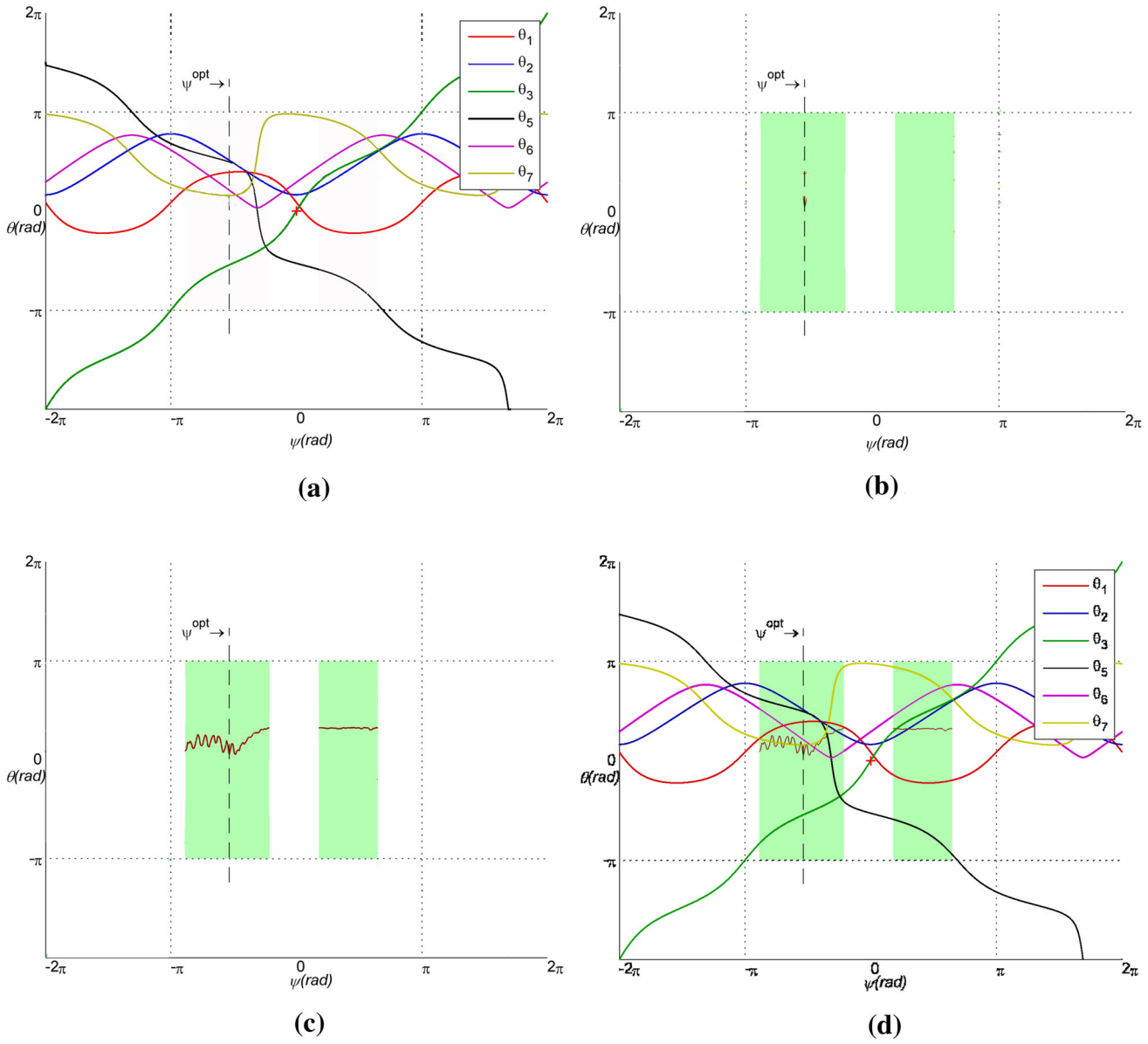

Fig. 5 Curves for the joints with respect to the arm angle and the feasible ranges for the arm angle, where the x-axis is ψ and the y-axis is θ_i, the *shadow region* denotes the final feasible values of ψ, the *waved lines* show the relationship between ψ and the value of the objective function, and the *cross* represents the point where $\psi = 0, \theta = 0$. **a** Curves for joints with respect to the arm angle. **b** Available range of arm angle. **c** Curves for the value of objective function with respect to the arm angle (**d**)

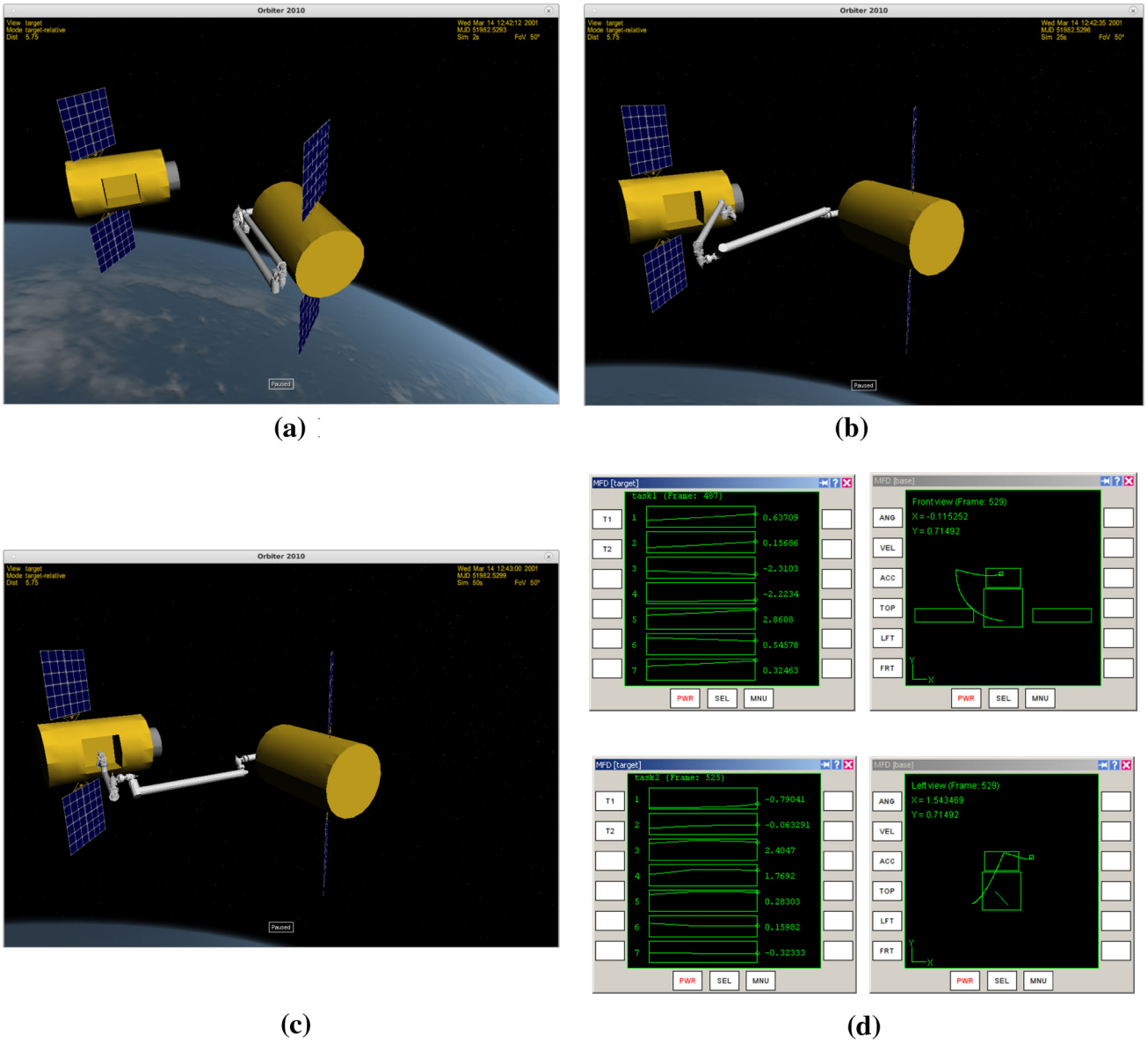

Fig. 6 3D motion simulation of the space manipulator developed based on ORBITER. **a** Initial state. **b** Unfolding state. **c** Observing state. **d** Geometric locus of motion

$[-159.454\ -38.216] \cup [32.143\ 116.769]^\circ$.

The final feasible ranges of ψ for the manipulator are shown in Fig. 5. Note that the set of feasible arm angles comprises two separate regions. It is impossible for the velocity-level to find all of the feasible values of ψ. However, our analytical approach can easily estimate all of the feasible regions and the solutions are extremely precise.

The optimal arm angle computed by the evaluation of $\delta \boldsymbol{q}$ for different values of ψ is

$$\psi^{\text{opt}} = -96.452.$$

The joint angles derived from ψ are

$[70.389\ 92.328\ -97.949\ 121.281\ 89.096\ 38.009\ 28.5831]^\circ$,

whereas the joint angles when $\psi = 0$ are

$[15.479\ 29.437\ 0\ 121.282\ -95.001\ 52.2726\ 175.764]^\circ$.

At this point, we note that there is no feasible value of ψ that can make θ_7 satisfy its limit, as shown in Fig. 5, where the cross represents the point where $\psi = 0, \theta = 0$.

The value of the objective function that corresponds to the optimal value of ψ is given by

$$\delta \boldsymbol{q}_{\text{opt}} = 0.1556.$$

The attitude angle of base satellite is

$$\boldsymbol{\omega}_{\varepsilon} = [\,17.029\ 5.658\ 1.632\,]^{\mathrm{T}\circ}.$$

Obviously, the changes in the attitude angle in the directions of the y-axis and x-axis are fairly small, where the only problems occur on the x-axis. An illustration of all these relationships is shown in Fig. 5. In the Fig. 5a, the curves represent the varying of seven joints with the arm angle under the condition of simulation parameters. Based on the maximum and minimum points of these curves, the possible value range of arm angle can be determined. The values of seven joints should be kept away from the values in the singular and extreme points. In the Fig. 5b, the green range represents the possible values of arm angle. We can take the values continuously from the range. What is more, the possible disturbance brought to the position and attitude of base is shown in Fig. 5c. Finally, the minimum point is taken as the global optimal solution of arm angle. Through reducing the possible range of arm angle and taking the seven parameters projected to one parameter, the computation is greatly reduced. The whole computation can be finished in a short time (a few seconds or more, more quickly than using the polynomial optimization).

Figure 5 shows the advantage of our proposed method, i.e., the solutions agree with the characteristics of the multi-solution for redundant manipulators. And we also developed a 3D visual simulation platform based on ORBITOR 2010. ORBITOR is a freeware space flight simulator program developed to simulate spaceflight using realistic Newtonian physics [27]. In this platform, the moving of the 7-DOF manipulator will be visualized. The simulation results showed that the movement of manipulator is smooth and the service-base is stable. The interface is shown as Fig. 6 which includes some illustrations of a space observation and maintenance task in space. In Fig. 6, there are two satellites: the left one is a target satellite, and the right one is a service satellite equipped with a 7-DOF manipulator. Figure 6a is the initial state while the service satellite is ready to start a maintenance task. Figure 6b and c show the motions, and the movement should make a minimized disturbance for the whole base. Our algorithm was mainly applied in this procedure. Figure 6d shows some detailed information which includes the angle value of seven joints and the motion curves of end-effector.

7 Discussion and summary

In this study, we proposed an analytical approach for obtaining all the feasible inverse kinematic solutions for space manipulators with joint and attitude limits, although its application has certain limitations. This method can only be used for some tasks where the manipulators actually manipulate part of the satellite itself. However, unlike the traditional method, our proposed approach can obtain the ranges of the feasible solutions for the 7-DOF manipulator as well as the maximum limit of the base disturbance, which results from the momentum conservation of the entire system. In terms of the efficiency of this approach, the joint parameterization approach plays a critical role that reduces the complex relationship between the joints into a simplified form. Only one parameter needs to be optimized to minimize the disturbance of the base; thus we only need constant time to execute the computation. The optimal computation allows us to avoid the semisingularity, which is a difficult problem to handle, although it has little effect.

Acknowledgments This work is supported by the Natural Science Foundation of Liaoning Province (No. 2013020007), the Program for Science and Technology Research in New Jinzhou District (No. 2013-GX1-015, KJCX-ZTPY-2014-0012).

References

1. Nanos K, Papadopoulos E (2011) On the use of free-floating space robots in the presence of angular momentum. Intell Serv Robot 4(1):3–15
2. Nenchev DN (1989) Redundancy resolution through local optimization: a review. J Robot Syst 6(6):769–798
3. Xu W, Liu Y, Liang B, Xu Y, Li C, Qiang W (2008) Non-holonomic path planning of a free-floating space robotic system using genetic algorithms. Adv Robot 22(4):451–476
4. Lee S, Bejczy A (1991) Redundant arm kinematic control based on parameterization. In: IEEE international conference on robotics and automation. IEEE, Sacramento, California, pp 458–465
5. Dahm P, Joublin F (1997) Closed form solution for the inverse kinematics of a redundant robot arm. Inst. Neuroinf, Ruhr Univ. Bochum, 44780, Bochum, Germany, Internal Rep 97–08
6. Moradi H, Lee S (2005) Joint limit analysis and elbow movement minimization for redundant manipulators using closed form method. Advances in intelligent computing. Springer, Berlin, pp 423–432
7. Asfour T, Dillmann R (2003) Human-like motion of a humanoid robot arm based on a closed-form solution of the inverse kinematics problem. In: Proceedings. 2003 IEEE/RSJ international conference on intelligent robots and systems, 2003 (IROS 2003), vol 2. IEEE, pp 1407–1412
8. Shimizu M, Yoon W-K, Kitagaki K (2007) A practical redundancy resolution for 7 DOF redundant manipulators with joint limits. In: 2007 IEEE international conference on robotics and automation. IEEE, pp 4510–4516
9. Shimizu M, Kakuya H, Yoon W-K, Kitagaki K, Kosuge K (2008) Analytical inverse kinematic computation for 7-DOF redundant manipulators with joint limits and its application to redundancy resolution. IEEE Trans Robot 24(5):1131–1142
10. Tolani D, Goswami A, Badler NI (2000) Real-time inverse kinematics techniques for anthropomorphic limbs. Graph Models 62(5):353–388
11. Singh GK, Claassens J (2010) An analytical solution for the inverse kinematics of a redundant 7DOF manipulator with link offsets. In: 2010 IEEE/RSJ international conference on intelligent robots and systems (IROS). IEEE, pp 2976–2982

12. Xie J, Yan S, Qiang W (2006) A method for solving the inverse kinematics problem of 6-DOF space manipulator. In: 1st international symposium on systems and control in aerospace and astronautics 2006 (ISSCAA 2006). IEEE, Harbin, pp 379–382
13. Kar I, Behera L (2010) Visual motor control of a 7 DOF robot manipulator using a fuzzy SOM network. Intell Serv Robot 3(1):49–60
14. Boudreau R, Podhorodeski RP (2010) Singularity analysis of a kinematically simple class of 7-jointed revolute manipulators. Trans Can Soc Mech Eng 34(1):105–117
15. Hollerbach JM (1985) Optimum kinematic design for a seven degree of freedom manipulator. In: Robotics research: the second international symposium. MIT Press, Cambridge, pp 215–222
16. Tondu B (2006) A closed-form inverse kinematic modelling of a 7R anthropomorphic upper limb based on a joint parametrization. In: 6th IEEE-RAS international conference on humanoid robots. IEEE, Toulouse Cedex 4, pp 390–397
17. Yu C, Jin M, Liu H (2012) An analytical solution for inverse kinematic of 7-DOF redundant manipulators with offset-wrist. In: International conference on mechatronics and automation (ICMA). IEEE, Harbin, pp 92–97
18. Taki Y, Sugimoto K (2003) Classification of singular configurations for 7-DOF manipulators with kinematic redundancy. In: Proceedings of 6th Japan–France congress on mechatronics and 4th Asia–Europe congress on mechatronics, pp 438–443
19. Park K-C, Chang P-H, Lee S (2002) A new kind of singularity in redundant manipulation: semi algorithmic singularity. In: IEEE international conference on robotics and automation 2002 (ICRA'02), vol 2. IEEE, Pittsburgh, pp 1979–1984
20. Chou JC (1992) Quaternion kinematic and dynamic differential equations. IEEE Trans Robot Autom 8(1):53–64
21. Yuan J (1988) Closed-loop manipulator control using quaternion feedback. IEEE J Robot Autom 4(4):434–440
22. Chen G, Jia Q, Sun H, Zhang X (2010) Non-holonomic path planning of space robot based on Newton iteration. In: 2010 IEEE proceedings of the 8th world congress on intelligent control and automation, Jinan, China, Jul 6–9, pp 6534–6538
23. Umetani Y, Yoshida K (1989) Resolved motion rate control of space manipulators with generalized Jacobian matrix. IEEE Trans Robot Autom 5(3):303–314
24. Huo X, Cheng Y, Wang Y, Hu Q (2011) PSO based trajectory planning of free floating space robot for minimizing spacecraft attitude disturbance. In: Control and decision conference (CCDC). IEEE, Mianyang, pp 819–822
25. Bae J-H, Park J-H, Oh Y, Kim D, Choi Y, Yang W (2015) Task space control considering passive muscle stiffness for redundant robotic arms. Intell Serv Robot 8(3):93–104
26. Yoshida K (1999) The SpaceDyn: a MATLAB toolbox for space and mobile robots. In: Proceedings. 1999 IEEE/RSJ international conference on intelligent robots and systems 1999 (IROS'99), vol 3. IEEE, pp 1633–1638
27. Schweiger M ORBITER. http://orbit.medphys.ucl.ac.uk/. Accessed 08 May 2015